arXiv:2004.01394v2 [hep-ex] 25 Apr 2020

First Measurements of $\chi_{cJ} \to \Sigma^-\bar{\Sigma}^+(J = 0, 1, 2)$ Decays

M. Ablikim[1], M. N. Achasov[10,d], P. Adlarson[64], S. Ahmed[15], M. Albrecht[4], A. Amoroso[63A,63C], Q. An[60,48], Anita[21], Y. Bai[47], O. Bakina[29], R. Baldini Ferroli[23A], I. Balossino[24A], Y. Ban[38,l], K. Begzsuren[26], J. V. Bennett[5], N. Berger[28], M. Bertani[23A], D. Bettoni[24A], F. Bianchi[63A,63C], J Biernat[64], J. Bloms[57], A. Bortone[63A,63C], I. Boyko[29], R. A. Briere[5], H. Cai[65], X. Cai[1,48], A. Calcaterra[23A], G. F. Cao[1,52], N. Cao[1,52], S. A. Cetin[51B], J. F. Chang[1,48], W. L. Chang[1,52], G. Chelkov[29,b,c], D. Y. Chen[6], G. Chen[1], H. S. Chen[1,52], M. L. Chen[1,48], S. J. Chen[36], X. R. Chen[25], Y. B. Chen[1,48], W. Cheng[63C], G. Cibinetto[24A], F. Cossio[63C], X. F. Cui[37], H. L. Dai[1,48], J. P. Dai[42,h], X. C. Dai[1,52], A. Dbeyssi[15], R. B. de Boer[4], D. Dedovich[29], Z. Y. Deng[1], A. Denig[28], I. Denysenko[29], M. Destefanis[63A,63C], F. De Mori[63A,63C], Y. Ding[34], C. Dong[37], J. Dong[1,48], L. Y. Dong[1,52], M. Y. Dong[1,48,52], S. X. Du[68], J. Fang[1,48], S. S. Fang[1,52], Y. Fang[1], R. Farinelli[24A,24B], L. Fava[63B,63C], F. Feldbauer[4], G. Felici[23A], C. Q. Feng[60,48], M. Fritsch[4], C. D. Fu[1], Y. Fu[1], X. L. Gao[60,48], Y. Gao[61], Y. Gao[38,l], Y. G. Gao[6], I. Garzia[24A,24B], E. M. Gersabeck[55], A. Gilman[56], K. Goetzen[11], L. Gong[37], W. X. Gong[1,48], W. Gradl[28], M. Greco[63A,63C], L. M. Gu[36], M. H. Gu[1,48], S. Gu[2], Y. T. Gu[13], C. Y Guan[1,52], A. Q. Guo[22], L. B. Guo[35], R. P. Guo[40], Y. P. Guo[9,i], Y. P. Guo[28], A. Guskov[29], S. Han[65], T. T. Han[41], T. Z. Han[9,i], X. Q. Hao[16], F. A. Harris[53], K. L. He[1,52], F. H. Heinsius[4], T. Held[4], Y. K. Heng[1,48,52], M. Himmelreich[11,g], T. Holtmann[4], Y. R. Hou[52], Z. L. Hou[1], H. M. Hu[1,52], J. F. Hu[42,h], T. Hu[1,48,52], Y. Hu[1], G. S. Huang[60,48], L. Q. Huang[61], X. T. Huang[41], Z. Huang[38,l], N. Huesken[57], T. Hussain[62], W. Ikegami Andersson[64], W. Imoehl[22], M. Irshad[60,48], S. Jaeger[4], S. Janchiv[26,k], Q. Ji[1], Q. P. Ji[16], X. B. Ji[1,52], X. L. Ji[1,48], H. B. Jiang[41], X. S. Jiang[1,48,52], X. Y. Jiang[37], J. B. Jiao[41], Z. Jiao[18], S. Jin[36], Y. Jin[54], T. Johansson[64], N. Kalantar-Nayestanaki[31], X. S. Kang[34], R. Kappert[31], M. Kavatsyuk[31], B. C. Ke[43,1], I. K. Keshk[4], A. Khoukaz[57], P. Kiese[28], R. Kiuchi[1], R. Kliemt[11], L. Koch[30], O. B. Kolcu[51B,f], B. Kopf[4], M. Kuemmel[4], M. Kuessner[4], A. Kupsc[64], M. G. Kurth[1,52], W. Kühn[30], J. J. Lane[55], J. S. Lange[30], P. Larin[15], L. Lavezzi[63C], H. Leithoff[28], M. Lellmann[28], T. Lenz[28], C. Li[39], C. H. Li[33], Cheng Li[60,48], D. M. Li[68], F. Li[1,48], G. Li[1], H. B. Li[1,52], H. J. Li[9,i], J. L. Li[41], J. Q. Li[4], Ke Li[1], L. K. Li[1], Lei Li[3], P. L. Li[60,48], P. R. Li[32], S. Y. Li[50], W. D. Li[1,52], W. G. Li[1], X. H. Li[60,48], X. L. Li[41], Z. B. Li[49], Z. Y. Li[49], H. Liang[60,48], H. Liang[1,52], Y. F. Liang[45], Y. T. Liang[25], L. Z. Liao[1,52], J. Libby[21], C. X. Lin[49], B. Liu[42,h], B. J. Liu[1], C. X. Liu[1], D. Liu[60,48], D. Y. Liu[42,h], F. H. Liu[44], Fang Liu[1], Feng Liu[6], H. B. Liu[13], H. M. Liu[1,52], Huanhuan Liu[1], Huihui Liu[17], J. B. Liu[60,48], J. Y. Liu[1,52], K. Liu[1], K. Y. Liu[34], Ke Liu[6], L. Liu[60,48], Q. Liu[52], S. B. Liu[60,48], Shuai Liu[46], T. Liu[1,52], X. Liu[32], Y. B. Liu[37], Z. A. Liu[1,48,52], Z. Q. Liu[41], Y. F. Long[38,l], X. C. Lou[1,48,52], H. J. Lu[18], J. D. Lu[1,52], J. G. Lu[1,48], X. L. Lu[1], Y. Lu[1], Y. P. Lu[1,48], C. L. Luo[35], M. X. Luo[67], P. W. Luo[49], T. Luo[9,i], X. L. Luo[1,48], S. Lusso[63C], X. R. Lyu[52], F. C. Ma[34], H. L. Ma[1], L. L. Ma[41], M. M. Ma[1,52], Q. M. Ma[1], R. Q. Ma[1,52], R. T. Ma[52], X. N. Ma[37], X. X. Ma[1,52], X. Y. Ma[1,48], Y. M. Ma[41], F. E. Maas[15], M. Maggiora[63A,63C], S. Maldaner[28], S. Malde[58], Q. A. Malik[62], A. Mangoni[23B], Y. J. Mao[38,l], Z. P. Mao[1], S. Marcello[63A,63C], Z. X. Meng[54], J. G. Messchendorp[31], G. Mezzadri[24A], T. J. Min[36], R. E. Mitchell[22], X. H. Mo[1,48,52], Y. J. Mo[6], N. Yu. Muchnoi[10,d], H. Muramatsu[56], S. Nakhoul[11,g], Y. Nefedov[29], F. Nerling[11,g], I. B. Nikolaev[10,d], Z. Ning[1,48], S. Nisar[8,j], S. L. Olsen[52], Q. Ouyang[1,48,52], S. Pacetti[23B], X. Pan[46], Y. Pan[55], A. Pathak[1], P. Patteri[23A], M. Pelizaeus[4], H. P. Peng[60,48], K. Peters[11,g], J. Pettersson[64], J. L. Ping[35], R. G. Ping[1,52], A. Pitka[4], R. Poling[56], V. Prasad[60,48], H. Qi[60,48], H. R. Qi[50], M. Qi[36], T. Y. Qi[2], S. Qian[1,48], W.-B. Qian[52], Z. Qian[49], C. F. Qiao[52], L. Q. Qin[12], X. P. Qin[13], X. S. Qin[4], Z. H. Qin[1,48], J. F. Qiu[1], S. Q. Qu[37], K. H. Rashid[62], K. Ravindran[21], C. F. Redmer[28], A. Rivetti[63C], V. Rodin[31], M. Rolo[63C], G. Rong[1,52], Ch. Rosner[15], M. Rump[57], A. Sarantsev[29,e], M. Savrié[24B], Y. Schelhaas[28], C. Schnier[4], K. Schoenning[64], D. C. Shan[46], W. Shan[19], X. Y. Shan[60,48], M. Shao[60,48], C. P. Shen[2], P. X. Shen[37], X. Y. Shen[1,52], H. C. Shi[60,48], R. S. Shi[1,52], X. Shi[1,48], X D Shi[60,48], J. J. Song[41], Q. Q. Song[60,48], W. M. Song[27], Y. X. Song[38,l], S. Sosio[63A,63C], S. Spataro[63A,63C], F. F. Sui[41], G. X. Sun[1], J. F. Sun[16], L. Sun[65], S. S. Sun[1,52], T. Sun[1,52], W. Y. Sun[35], Y. J. Sun[60,48], Y. K Sun[60,48], Y. Z. Sun[1], Z. T. Sun[1], Y. H. Tan[65], Y. X. Tan[60,48], C. J. Tang[45], G. Y. Tang[1], J. Tang[49], V. Thoren[64], B. Tsednee[26], I. Uman[51D], B. Wang[1], B. L. Wang[52], C. W. Wang[36], D. Y. Wang[38,l], H. P. Wang[1,52], K. Wang[1,48], L. L. Wang[1], M. Wang[41], M. Z. Wang[38,l], Meng Wang[1,52], W. H. Wang[65], W. P. Wang[60,48], X. Wang[38,l], X. F. Wang[32], X. L. Wang[9,i], Y. Wang[49], Y. Wang[60,48], Y. D. Wang[15], Y. F. Wang[1,48,52], Y. Q. Wang[1], Z. Wang[1,48], Z. Y. Wang[1], Ziyi Wang[52], Zongyuan Wang[1,52], T. Weber[4], D. H. Wei[12], P. Weidenkaff[28], F. Weidner[57], S. P. Wen[1], D. J. White[55], U. Wiedner[4], G. Wilkinson[58], M. Wolke[64], L. Wollenberg[4], J. F. Wu[1,52], L. H. Wu[1], L. J. Wu[1,52], X. Wu[9,i], Z. Wu[1,48], L. Xia[60,48], H. Xiao[9,i], S. Y. Xiao[1], Y. J. Xiao[1,52], Z. J. Xiao[35], X. H. Xie[38,l], Y. G. Xie[1,48], Y. H. Xie[6], T. Y. Xing[1,52], X. A. Xiong[1,52], G. F. Xu[1], J. J. Xu[36], Q. J. Xu[14], W. Xu[1,52], X. P. Xu[46], L. Yan[9,i], L. Yan[63A,63C], W. B. Yan[60,48], W. C. Yan[68], Xu Yan[46], H. J. Yang[42,h], H. X. Yang[1], L. Yang[65], R. X. Yang[60,48], S. L. Yang[1,52], Y. H. Yang[36], Y. X. Yang[12], Yifan Yang[1,52], Zhi Yang[25], M. Ye[1,48], M. H. Ye[7], J. H. Yin[1], Z. Y. You[49], B. X. Yu[1,48,52], C. X. Yu[37], G. Yu[1,52], J. S. Yu[20,m], T. Yu[61], C. Z. Yuan[1,52], W. Yuan[63A,63C], X. Q. Yuan[38,l], Y. Yuan[1], Z. Y. Yuan[49], C. X. Yue[33], A. Yuncu[51B,a], A. A. Zafar[62], Y. Zeng[20,m], B. X. Zhang[1], Guangyi Zhang[16], H. H. Zhang[49], H. Y. Zhang[1,48], J. L. Zhang[66], J. Q. Zhang[4], J. W. Zhang[1,48,52], J. Y. Zhang[1], J. Z. Zhang[1,52], Jianyu Zhang[1,52], Jiawei Zhang[1,52], L. Zhang[1], Lei Zhang[36], S. Zhang[49], S. F. Zhang[36], T. J. Zhang[42,h], X. Y. Zhang[41], Y. Zhang[58], Y. H. Zhang[1,48], Y. T. Zhang[60,48], Yan Zhang[60,48], Yao Zhang[1], Yi Zhang[9,i], Z. H. Zhang[6], Z. Y. Zhang[65], G. Zhao[1], J. Zhao[33], J. Y. Zhao[1,52], J. Z. Zhao[1,48], Lei Zhao[60,48], Ling Zhao[1], M. G. Zhao[37], Q. Zhao[1], S. J. Zhao[68], Y. B. Zhao[1,48], Y. X. Zhao Zhao[25], Z. G. Zhao[60,48], A. Zhemchugov[29,b], B. Zheng[61], J. P. Zheng[1,48], Y. Zheng[38,l], Y. H. Zheng[52], B. Zhong[35], C. Zhong[61], L. P. Zhou[1,52], Q. Zhou[1,52], X. Zhou[65], X. K. Zhou[52], X. R. Zhou[60,48], A. N. Zhu[1,52], J. Zhu[37], K. Zhu[1], K. J. Zhu[1,48,52], S. H. Zhu[59], W. J. Zhu[37], X. L. Zhu[50], Y. C. Zhu[60,48], Z. A. Zhu[1,52], B. S. Zou[1], J. H. Zou[1]

(BESIII Collaboration)

[1] *Institute of High Energy Physics, Beijing 100049, People's Republic of China*

[2] *Beihang University, Beijing 100191, People's Republic of China*
[3] *Beijing Institute of Petrochemical Technology, Beijing 102617, People's Republic of China*
[4] *Bochum Ruhr-University, D-44780 Bochum, Germany*
[5] *Carnegie Mellon University, Pittsburgh, Pennsylvania 15213, USA*
[6] *Central China Normal University, Wuhan 430079, People's Republic of China*
[7] *China Center of Advanced Science and Technology, Beijing 100190, People's Republic of China*
[8] *COMSATS University Islamabad, Lahore Campus, Defence Road, Off Raiwind Road, 54000 Lahore, Pakistan*
[9] *Fudan University, Shanghai 200443, People's Republic of China*
[10] *G.I. Budker Institute of Nuclear Physics SB RAS (BINP), Novosibirsk 630090, Russia*
[11] *GSI Helmholtzcentre for Heavy Ion Research GmbH, D-64291 Darmstadt, Germany*
[12] *Guangxi Normal University, Guilin 541004, People's Republic of China*
[13] *Guangxi University, Nanning 530004, People's Republic of China*
[14] *Hangzhou Normal University, Hangzhou 310036, People's Republic of China*
[15] *Helmholtz Institute Mainz, Johann-Joachim-Becher-Weg 45, D-55099 Mainz, Germany*
[16] *Henan Normal University, Xinxiang 453007, People's Republic of China*
[17] *Henan University of Science and Technology, Luoyang 471003, People's Republic of China*
[18] *Huangshan College, Huangshan 245000, People's Republic of China*
[19] *Hunan Normal University, Changsha 410081, People's Republic of China*
[20] *Hunan University, Changsha 410082, People's Republic of China*
[21] *Indian Institute of Technology Madras, Chennai 600036, India*
[22] *Indiana University, Bloomington, Indiana 47405, USA*
[23] *(A)INFN Laboratori Nazionali di Frascati, I-00044, Frascati, Italy; (B)INFN and University of Perugia, I-06100, Perugia, Italy*
[24] *(A)INFN Sezione di Ferrara, I-44122, Ferrara, Italy; (B)University of Ferrara, I-44122, Ferrara, Italy*
[25] *Institute of Modern Physics, Lanzhou 730000, People's Republic of China*
[26] *Institute of Physics and Technology, Peace Ave. 54B, Ulaanbaatar 13330, Mongolia*
[27] *Jilin University, Changchun 130012, People's Republic of China*
[28] *Johannes Gutenberg University of Mainz, Johann-Joachim-Becher-Weg 45, D-55099 Mainz, Germany*
[29] *Joint Institute for Nuclear Research, 141980 Dubna, Moscow region, Russia*
[30] *Justus-Liebig-Universitaet Giessen, II. Physikalisches Institut, Heinrich-Buff-Ring 16, D-35392 Giessen, Germany*
[31] *KVI-CART, University of Groningen, NL-9747 AA Groningen, The Netherlands*
[32] *Lanzhou University, Lanzhou 730000, People's Republic of China*
[33] *Liaoning Normal University, Dalian 116029, People's Republic of China*
[34] *Liaoning University, Shenyang 110036, People's Republic of China*
[35] *Nanjing Normal University, Nanjing 210023, People's Republic of China*
[36] *Nanjing University, Nanjing 210093, People's Republic of China*
[37] *Nankai University, Tianjin 300071, People's Republic of China*
[38] *Peking University, Beijing 100871, People's Republic of China*
[39] *Qufu Normal University, Qufu 273165, People's Republic of China*
[40] *Shandong Normal University, Jinan 250014, People's Republic of China*
[41] *Shandong University, Jinan 250100, People's Republic of China*
[42] *Shanghai Jiao Tong University, Shanghai 200240, People's Republic of China*
[43] *Shanxi Normal University, Linfen 041004, People's Republic of China*
[44] *Shanxi University, Taiyuan 030006, People's Republic of China*
[45] *Sichuan University, Chengdu 610064, People's Republic of China*
[46] *Soochow University, Suzhou 215006, People's Republic of China*
[47] *Southeast University, Nanjing 211100, People's Republic of China*
[48] *State Key Laboratory of Particle Detection and Electronics, Beijing 100049, Hefei 230026, People's Republic of China*
[49] *Sun Yat-Sen University, Guangzhou 510275, People's Republic of China*
[50] *Tsinghua University, Beijing 100084, People's Republic of China*
[51] *(A)Ankara University, 06100 Tandogan, Ankara, Turkey; (B)Istanbul Bilgi University, 34060 Eyup, Istanbul, Turkey; (C)Uludag University, 16059 Bursa, Turkey; (D)Near East University, Nicosia, North Cyprus, Mersin 10, Turkey*
[52] *University of Chinese Academy of Sciences, Beijing 100049, People's Republic of China*
[53] *University of Hawaii, Honolulu, Hawaii 96822, USA*
[54] *University of Jinan, Jinan 250022, People's Republic of China*
[55] *University of Manchester, Oxford Road, Manchester, M13 9PL, United Kingdom*
[56] *University of Minnesota, Minneapolis, Minnesota 55455, USA*
[57] *University of Muenster, Wilhelm-Klemm-Str. 9, 48149 Muenster, Germany*
[58] *University of Oxford, Keble Rd, Oxford, UK OX13RH*
[59] *University of Science and Technology Liaoning, Anshan 114051, People's Republic of China*
[60] *University of Science and Technology of China, Hefei 230026, People's Republic of China*
[61] *University of South China, Hengyang 421001, People's Republic of China*
[62] *University of the Punjab, Lahore-54590, Pakistan*
[63] *(A)University of Turin, I-10125, Turin, Italy; (B)University of Eastern Piedmont, I-15121, Alessandria, Italy; (C)INFN,*

I-10125, Turin, Italy
[64] Uppsala University, Box 516, SE-75120 Uppsala, Sweden
[65] Wuhan University, Wuhan 430072, People's Republic of China
[66] Xinyang Normal University, Xinyang 464000, People's Republic of China
[67] Zhejiang University, Hangzhou 310027, People's Republic of China
[68] Zhengzhou University, Zhengzhou 450001, People's Republic of China

[a] Also at Bogazici University, 34342 Istanbul, Turkey
[b] Also at the Moscow Institute of Physics and Technology, Moscow 141700, Russia
[c] Also at the Functional Electronics Laboratory, Tomsk State University, Tomsk, 634050, Russia
[d] Also at the Novosibirsk State University, Novosibirsk, 630090, Russia
[e] Also at the NRC "Kurchatov Institute", PNPI, 188300, Gatchina, Russia
[f] Also at Istanbul Arel University, 34295 Istanbul, Turkey
[g] Also at Goethe University Frankfurt, 60323 Frankfurt am Main, Germany
[h] Also at Key Laboratory for Particle Physics, Astrophysics and Cosmology, Ministry of Education; Shanghai Key Laboratory for Particle Physics and Cosmology; Institute of Nuclear and Particle Physics, Shanghai 200240, People's Republic of China
[i] Also at Key Laboratory of Nuclear Physics and Ion-beam Application (MOE) and Institute of Modern Physics, Fudan University, Shanghai 200443, People's Republic of China
[j] Also at Harvard University, Department of Physics, Cambridge, MA, 02138, USA
[k] Currently at: Institute of Physics and Technology, Peace Ave.54B, Ulaanbaatar 13330, Mongolia
[l] Also at State Key Laboratory of Nuclear Physics and Technology, Peking University, Beijing 100871, People's Republic of China
[m] School of Physics and Electronics, Hunan University, Changsha 410082, China

We measured the branching fractions of the decays $\chi_{cJ} \to \Sigma^-\bar{\Sigma}^+$ for the first time using the final states $n\bar{n}\pi^+\pi^-$. The data sample exploited here is 448.1×10^6 $\psi(3686)$ events collected with BESIII. We find $\mathcal{B}(\chi_{cJ} \to \Sigma^-\bar{\Sigma}^+) = (51.3\pm2.4\pm4.1)\times10^{-5}$, $(5.7\pm1.4\pm0.6)\times10^{-5}$, and $(4.4\pm1.7\pm0.5)\times10^{-5}$, for $J = 0, 1, 2$, respectively, where the first uncertainties are statistical and the second systematic.

PACS numbers: 13.20.Gd, 13.25.Gv, 14.40.Pq

I. INTRODUCTION

Experimental studies of the $\chi_{cJ}(J = 0, 1, 2)$ states are important for testing models that are based on non-perturbative Quantum Chromodynamics (QCD). The χ_{cJ} mesons are P-wave $c\bar{c}$ triple-states with a spin parity J^{++}, and cannot be produced directly in e^+e^- annihilation. However, they can be produced in the radiative decays of the vector charmonium state $\psi(3686)$ with considerable branching fractions (BFs) of $\sim 9\%$ [1]. A large sample of $\psi(3686)$ decays has been collected at BESIII, which provides a good opportunity to investigate the P-wave χ_{cJ} states [2].

Many theoretical calculations show that the color octet mechanism (COM) could have a large contribution in describing P-wave quarkonium decays [3–5]. The predictions for χ_{cJ} decays to meson pairs are in agreement with the experimental results [6], while contradictions are observed in the χ_{cJ} decays to baryon pairs ($B\bar{B}$) [4, 5]. For example, the predicted BFs of $\chi_{cJ} \to \Lambda\bar{\Lambda}$ disagree with measured values [7]. In addition, the study of $\chi_{c0} \to B\bar{B}$ is helpful to test the validity of the helicity selection rule (HSR) [8, 9], which prohibits $\chi_{c0} \to B\bar{B}$. Measured BFs for $\chi_{c0} \to p\bar{p}$, $\Lambda\bar{\Lambda}$ and $\Xi^-\bar{\Xi}^+$ do not vanish [7, 10], demonstrating a strong violation of HSR in charmonium decay. The quark creation model (QCM) [11] is developed to explain the strengthened decays of $\chi_{c0} \to B\bar{B}$ and it predicts the rate of $\chi_{c0,2} \to \Xi^+\Xi^-$ [10] well. However, the same model is unable to accurately reproduce the observed decay rates to other $B\bar{B}$ final states [7]. Recent BF data for $\chi_{c1,2} \to \Sigma^+\bar{\Sigma}^-$ and $\Sigma^0\bar{\Sigma}^0$ [12] are in good agreement with COM predictions [4], while measured BFs of $\chi_{c0} \to \Sigma^+\bar{\Sigma}^-$ and $\Sigma^0\bar{\Sigma}^0$ [12, 13] are inconsistent with COM models based on the charm-meson-loop mechanism [5, 14], and violate the HSR, too. Experimentally, there are no BF data of $\chi_{cJ} \to \Sigma^-\bar{\Sigma}^+$, and therefore those measurements are necessary to further test the validity of COM, HSR and QCM.

In this paper, we report on an analysis of the processes $\psi(3686) \to \gamma\chi_{cJ}$, $\chi_{cJ} \to \Sigma^-\bar{\Sigma}^+$ ($\Sigma^- \to n\pi^-$, $\bar{\Sigma}^+ \to \bar{n}\pi^+$) using a data sample of $(448.1 \pm 2.9) \times 10^6$ $\psi(3686)$ events collected with BESIII [15]. The BFs of the decays $\chi_{cJ} \to \Sigma^-\bar{\Sigma}^+$ are measured for the first time.

II. BESIII DETECTOR AND MONTE CARLO SIMULATION

The BESIII detector operating at the Beijing electron-positron collider (BEPCII), is a double-ring e^+e^- collider with a peak luminosity of 1×10^{33} cm^{-2}s^{-1} at center-of-mass energy $\sqrt{s} = 3.77$ GeV [2, 16]. The BESIII detector has a geometrical acceptance of 93% over 4π solid angle. The cylindrical core of the BESIII detector consists of a small-cell, helium-gas-based (60% He, 40% C_3H_8) main drift chamber (MDC) which is used to track the charged particles. The MDC is surrounded by a time-of-flight (TOF) system built from plastic scintillators that is used for charged-particle identification (PID). Photons are detected and their energies and positions are measured with

an electromagnetic calorimeter (EMC) consisting of 6240 CsI(TI) crystals. The sub-detectors are enclosed in a superconducting solenoid magnet with a field strength of 1 T. Outside the magnet coil, the muon detector consists of 1000 m^2 resistive plate chambers in nine barrel and eight end-cap layers, providing a spatial resolution of better than 2 cm. The momentum resolution of charged particle is 0.5% at 1 GeV. The energy loss (dE/dx) measurement provided by the MDC has a resolution of 6%, and the time resolution of the TOF is 80 ps (110 ps) in the barrel (end-caps). The energy resolution for photons is 2.5% (5%) at 1 GeV in the barrel (end-caps) of the EMC.

A dedicated Monte Carlo (MC) simulation of the BESIII detector based on GEANT4 [17] is used for the optimization of event selection criteria, the determination of the detection efficiencies, and to estimate the contributions of backgrounds. A generic MC sample with 5.06×10^8 events is generated, where the production of the $\psi(3686)$ resonance is simulated by the MC event generator KKMC [18]. Particle decays are generated by EVTGEN [19] for the known decay modes with BFs taken from Particle Data Group (PDG), and by LUNDCHARM [20] for the remaining unknown decays. For the MC simulation of the signal process, the decay of $\psi(3686) \to \gamma\chi_{cJ}$ is generated by following the angular distributions taken from Ref. [21], where the polar angles θ of radiation photons are distributed according to $(1+\cos^2\theta), (1-\frac{1}{3}\cos^2\theta), (1+\frac{1}{13}\cos^2\theta)$ for $J = 0,\ 1,\ 2$. The $\chi_{cJ} \to \Sigma^-\bar{\Sigma}^+$ decays are generated with the ANGSAM [19] model, with helicity angles of the Σ satisfying the angular distribution $1+\alpha\cos^2\theta$. Note that $\alpha = 0$ for the decay of the χ_{c0} because the helicity angular distribution of a scalar particle is isotropic. The subsequent decays $\Sigma^- \to n\pi^-$ and $\bar{\Sigma}^+ \to \bar{n}\pi^+$ are generated with uniform momentum distribution in the phase space (PHSP) [22].

III. EVENT SELECTION AND BACKGROUND ANALYSIS

We reconstruct the candidate events from the decay chain $\psi(3686) \to \gamma\chi_{cJ}$ followed by $\chi_{cJ} \to \Sigma^-\bar{\Sigma}^+$ with subsequent decays $\Sigma^- \to n\pi^-$ and $\bar{\Sigma}^+ \to \bar{n}\pi^+$. The charged tracks are reconstructed with the hit information from the MDC. The polar angles of charged tracks in the MDC have to fulfill $|\cos\theta| < 0.93$. A loose vertex requirement is applied for charged-track candidates to implement the sizable decay lengths of Σ^- and $\bar{\Sigma}^+$, and each charged track is required to have a point of closest approach to e^+e^- interaction point that is within 10 cm in the plane perpendicular to the beam axis and within $\pm$30 cm in the beam direction. The combined information of dE/dx and TOF is used to calculate PID probabilities for the pion, kaon and proton hypothesis, respectively, and the particle type with the highest probability is assigned to the corresponding track. In this analysis, candidate events are required to have two charged tracks identified as π^+ and π^-.

There are three neutral particles in the final states of the signal process, the radiative photon γ, anti-neutron $\bar{n}$ and neutron n. The radiative photon deposits most of its energy in the EMC with a high efficiency. The $\bar{n}$ annihilates in the EMC and produces several secondary particles with a total energy deposition up to 2 GeV. The n, on the other hand, is not identifiable due to its low interaction efficiency and its small energy deposition. Therefore, the $\bar{n}$ and radiative photon are selected in this process. The most energetic shower in the EMC is assigned to be the $\bar{n}$ candidate. To discriminate $\bar{n}$ from photons and to suppress the electronic noise, several selection criteria are used. Firstly, the deposited energy of $\bar{n}$ is required to be in the range 0.2$-$2.0 GeV. Secondly, the second moment of candidate shower, defined as $S = \sum_i E_i r_i^2 / \sum_i E_i$, must satisfy $S > 20$ cm^2, where E_i is the energy deposited in the i^{th} crystal of the shower and r_i is the distance from the center of that crystal to the center of the shower [23]. Furthermore, the number of EMC hits in a 40° cone seen from the vertex around the $\bar{n}$ shower direction is required to be greater than 20. After applying these selection criteria, the $\bar{n}$ candidates have a purity of more than 98% estimated from signal MC sample.

To avoid the secondary showers originating from $\bar{n}$ annihilation, the radiative photon is selected from EMC showers that have an opening angle with respect to the $\bar{n}$ direction that is greater than 40°. Good photon candidates are selected by requiring a minimum energy deposition of 80 MeV in the EMC, and are isolated from all charged tracks by a minimum angle of 10°. The time information of the EMC is used to further suppress electronic noise and energy depositions unrelated to the event. At least one good photon candidate is required in an event.

The momentum or direction information of candidate particles are subjected to a kinematic fit that assumes the $\psi(3686) \to \gamma n\bar{n}\pi^+\pi^-$ hypothesis, where the direction of $\bar{n}$ in the fit is involved and n is treated as a missing particle. The kinematic fit is then applied by imposing energy and momentum conservation at the IP and by constraining the $\bar{n}\pi^+$ invariant mass to match the nominal $\bar{\Sigma}^+$ mass [1]. For events with more than one photon candidate, the combination with a minimum $\chi^2_{\rm kfit}$ is chosen with the requirement that $\chi^2_{\rm kfit} < 20$.

After applying the kinematic fit, the backgrounds from $\psi(3686) \to \pi^0\pi^0 J/\psi$ followed by decays of $J/\psi \to B\bar{B}$ and $\pi^0 \to \gamma\gamma$ are suppressed by reconstructing events with two photon candidates. An event is then discarded when the invariant mass of any two photons are located within 120 MeV/c^2 and 150 MeV/c^2. The contamination of the channel $\psi(3686) \to \pi^+\pi^- J/\psi$ with $J/\psi \to n\bar{n}$ is removed by requiring $|M_{\rm rec}(\pi^+\pi^-) - m(J/\psi)| > 10$ MeV/c^2, where $M_{\rm rec}(\pi^+\pi^-)$ is the recoil mass of the $\pi^+\pi^-$ pair and $m(J/\psi)$ is the world average mass of the J/ψ meson [1]. Another sources of backgrounds are from

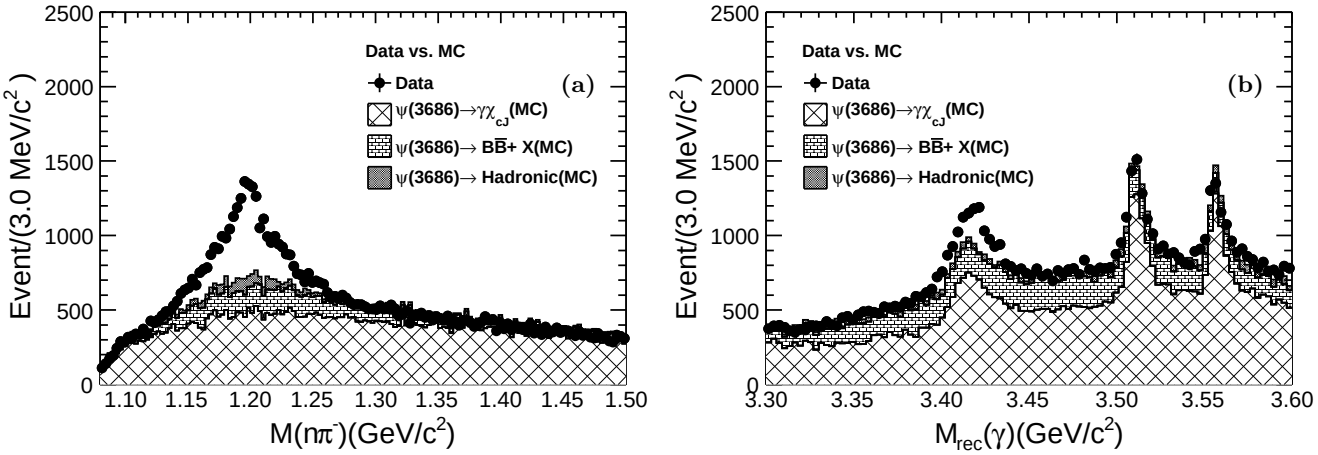


FIG. 1. Invariant-mass distributions of reconstructed Σ^- candidates (a) and the recoil mass of γ (b). The dots with error bars denote the data. The contributions for each component are obtained using MC simulations and are indicated as the hatched histograms.

events containing a K^0_S. These events are removed by requiring $|M(\pi^+\pi^-) - m(K^0_S)| > 10$ MeV/c^2, whereby $M(\pi^+\pi^-)$ and $m(K^0_S)$ are the reconstructed $\pi^+\pi^-$ invariant mass and world average mass of the K^0_S [1], respectively. The signal could be contaminated with background from $\psi(3686) \to \Sigma^-\bar{\Sigma}^+$ whereby one fake photon has been reconstructed. To remove such background, events are rejected for which the $\chi^2_{\rm kfit}(\Sigma^-\bar{\Sigma}^+)$ is smaller than $\chi^2_{\rm kfit}(\gamma\Sigma^-\bar{\Sigma}^+)$.

The invariant-mass spectrum of $n\pi^-$ and the recoil mass spectrum of the γ are shown in Fig. 1 for both data and MC simulations, where Σ^- and χ_{cJ} signals can be observed. The MC results represent the main characteristics of the various background sources. However, they cannot fully describe the data due to missing or improper modeling of background processes involving $B\bar{B}$, especially when the final states contain $n\bar{n}$. Using the topology technique [24], we have categorized the main background sources into three kinds: a) the process $\psi(3686) \to \gamma\chi_{cJ}$ whereby the χ_{cJ} decays to hadronic final states, which shows a peak in $M_{\rm rec}(\gamma)$ and no peaking structure in $M(n\pi^-)$; b) the process $\psi(3686) \to B\bar{B}$ or $J/\psi \to B\bar{B}$ via the hadronic transition from $\psi(3686)$, which is not peaking in $M_{\rm rec}(\gamma)$ but shows a wide bump in $M(n\pi^-)$; c) the decays $\psi(3686)$ to hadronic final states, which are non-peaking in both $M_{\rm rec}(\gamma)$ and $M(n\pi^-)$. Besides, a two-dimensional (2D) distribution of $M(n\pi^-)$ and $M_{\rm rec}(\gamma)$ is shown in Fig. 2 for the data. Clear accumulations of candidate events of the signal process $\chi_{c0} \to \Sigma^-\bar{\Sigma}^+$ are observed around the intersections of the χ_{c0} and Σ^- mass regions, and a signature of the process $\chi_{c1,2} \to \Sigma^-\bar{\Sigma}^+$ can be observed. A data sample corresponding to an integrated luminosity of 44 pb^{-1}, taken at $\sqrt{s} = 3.65$ GeV, is used to estimate the continuum background arising from quantum electrodynamics (QED) processes. No peaking backgrounds are observed in the mass spectrum of $M_{\rm rec}(\gamma)$ for the continuum data sample, therefore the contribution from QED background can be neglected.

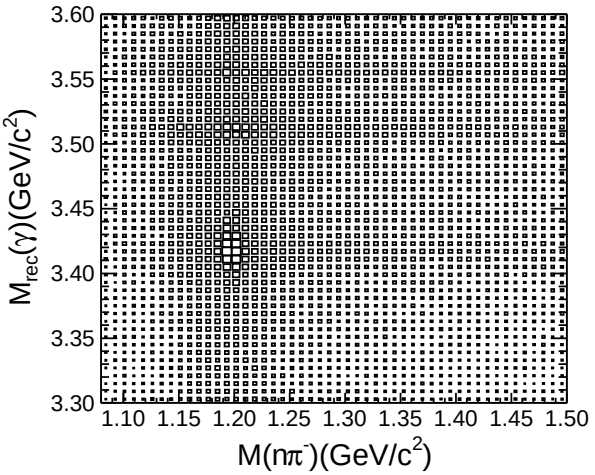


FIG. 2. A 2D distribution of $M_{\rm rec}(\gamma)$ versus $M(n\pi^-)$ for data.

IV. EXTRACTION OF THE SIGNAL

To extract the signal yields for $\chi_{cJ} \to \Sigma^-\bar{\Sigma}^+$, unbinned maximum-likelihood fits to the $M_{\rm rec}(\gamma)$ distributions as a function of $M(n\pi^-)$ are performed, noted as bin-by-bin fit. The bin width for $M(n\pi^-)$ is determined by testing the MC samples, where the MC samples include events from MC-generated background sources, and events randomly sampled from signal MC events with the same amount events as observed in data as signal. The bin width is determined when the minimum input-output difference is obtained for the extraction of the signal and it is found to be 10 MeV/c^2.

In the fit of $M_{\rm rec}(\gamma)$ in each $n\pi^-$ bin, the χ_{cJ} signals are described by the MC shapes convoluted with

Gaussian functions to compensate for a possible resolution difference between the data and MC. For a proper modeling of the lineshape of the signal, thereby suppressing photon misidentification, we selected signal MC events for which the opening angle of the reconstructed photon matches the value given by the generator. A second-order Chebychev polynomial function is used to describe the non-χ_{cJ} background. It should be noted that the $M_{\rm rec}(\gamma)$ resolution of the process $\psi(3686) \to \gamma\chi_{cJ}$, with inclusive decays of the χ_{cJ}, is the same as observed in the signal MC data. Figure 3 shows the results of a bin-by-bin fit of one of the $M_{\rm rec}(\gamma)$ distributions selected for a bin in $M(n\pi^-)$ at the Σ^- peak position. Figure 4 shows the fitted signal yields of $\psi(3686) \to \gamma\chi_{cJ}$ as a function of $M(n\pi^-)$. Clear signatures of Σ^- decays can be observed. Binned least-χ^2 fits are subsequently performed to these spectra. The signal shapes are described by MC-simulated responses convoluted with Gaussian distributions and backgrounds are described by second-order Chebychev polynomials. The fit results are shown by the lines in Fig. 4. The statistical significances of the signal for the three χ_{cJ} cases are found to be 30σ, 5.8σ and 3.6σ, respectively. The significances are calculated from the χ^2 differences between fits with and without the signal processes. The corresponding signal yields are summarized in Table I. The BFs are obtained from:

$$\mathcal{B}(\chi_{cJ} \to \Sigma^-\bar{\Sigma}^+) = \frac{N^{obs}}{N_{\psi(3686)} \cdot \epsilon \cdot \prod \mathcal{B}_i}\ , \qquad (1)$$

where N^{obs} is the number of signal events obtained from the bin-by-bin fit; ϵ is the detection efficiency obtained from signal MC after the photon matching; $\prod \mathcal{B}_i$ is the product of BFs for the $\psi(3686) \to \gamma\chi_{cJ}$, $\Sigma^- \to n\pi^-$ and $\bar{\Sigma}^+ \to \bar{n}\pi^+$ channels; and $N_{\psi(3686)}$ is the total number of $\psi(3686)$ events. The corresponding detection efficiencies and the resultant BFs are summarized in Table I. We note that due to the low-energy radiative photon of χ_{cJ} ($J = 1, 2$), the detection efficiency tends to get smaller due to the rejection of π^0-mass requirement.

V. ESTIMATION OF SYSTEMATIC UNCERTAINTIES

Various sources of systematic uncertainties are studied and summarized in Table II. The investigated uncertainties are discussed in detail in the following:

a. MDC Tracking: The tracking efficiencies for π^+/π^- as functions of the transverse momentum have been studied with the process $J/\psi \to \Sigma^{*-}\bar{\Sigma}^+ \to \pi^-\Lambda\ \bar{n}\ \pi^+(\Lambda \to \pi^- p)$. The efficiency difference between data and MC is 1.4% for each charged-pion track.

b. Photon Reconstruction: The uncertainty of the photon-detection efficiency is estimated to be 1.0% per photon [25].

c. $\bar{n}$ Selection and Kinematic Fit: The systematic uncertainties of the $\bar{n}$ selection and the kinematic fit involving the $\bar{n}$ is studied using the control sample of $J/\psi \to \Sigma^*\bar{\Sigma}^+$. The relative difference of 5.8% in efficiency between MC and data is assigned as the corresponding systematic uncertainty.

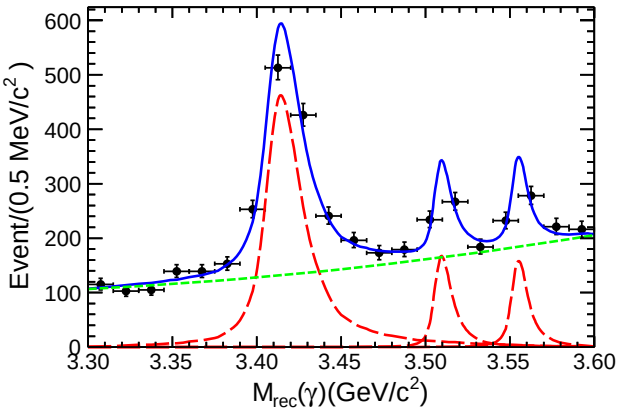


FIG. 3. Fit to the $M_{\rm rec}(\gamma)$ distribution at the maximum accumulation in the $M(n\pi^-)$ bin. Black dots with error bars are from data, the solid blue lines are the best fit result, dashed red lines represent signal contributions, and dashed green lines are the fitted backgrounds.

d. Mass Window Requirement: Various cuts in the mass spectra have been used to select events, namely on $M(\gamma\gamma)$, $M(\pi^+\pi^-)$ and $M_{rec.}(\pi^+\pi^-)$. Cross checks of systematic effects for these mass window requirements are considered following the procedure described in Ref. [26]. The consistency of the results is checked by comparing the uncorrelated differences between the parameter values, $x_{test} \pm \sigma_{test}$, obtained from the fits to the nominal results, $x_{nom.} \pm \sigma_{nom.}$. The systematic sources cannot be discarded when the significance of uncorrelated differences, $\Delta x_{uncor.} = |x_{nom.} - x_{test}|/\sqrt{|\sigma^2_{nom.} - \sigma^2_{test}|} > 2$. By comparing the results of various selections taken within a proper range with the nominal result, the one with the largest difference is taken as an estimate of the corresponding uncertainty. For the χ_{c0} case, the π^0 veto is tested by varying the rejection windows, $|M(\gamma\gamma) - m(\pi^0)|$ from 3 to 18 MeV/c^2. The largest deviation $\Delta x_{uncor.}$ is found when the veto is applied at 12 MeV/c^2. Similar attempts are performed for the mass windows of $M_{\rm rec}(\pi^+\pi^-)$ and M$(\pi^+\pi^-)$. The largest deviations are found when the windows are $|M_{\rm rec}(\pi^+\pi^-) - m(J/\psi)| > 16$ MeV/c^2 and $|M(\pi^+\pi^-)$ - $m(\mathrm{K^0_S})| > 12$ MeV/c^2. The differences to the nominal results are then taken as an estimate of the systematic uncertainty. In all cases, we observe no tendency of $\Delta x_{uncor.}$ along with the selection variations, indicating no bias in these selection criteria. For $\chi_{c1,2}$, it is found that the $\Delta x_{uncor.}$ for all the tests are less than 2σ. Therefore, no systematic uncertainties are considered in that case.

e. Fitting Process: To estimate the uncertainties from the fitting process, the following three studies are made.

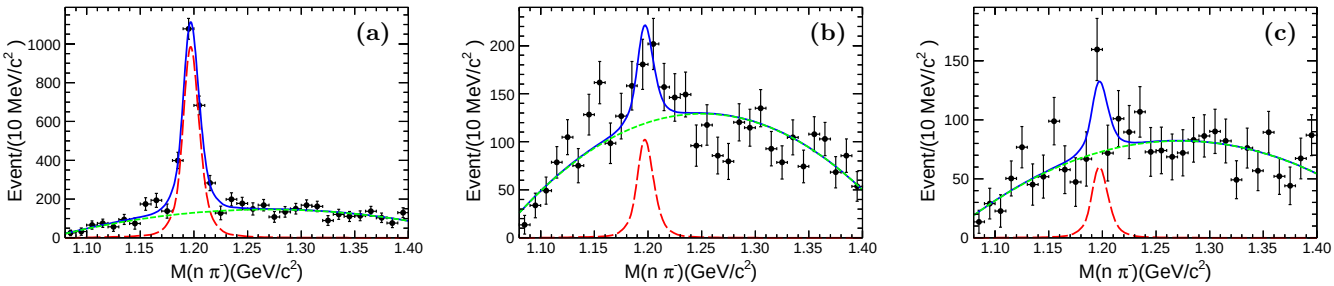


FIG. 4. The $\chi_{cJ} \to \Sigma^-\bar{\Sigma}^+$ signal yields as a function of $M(n\pi^-)$ for (a) χ_{c0} (b) χ_{c1} and (c) χ_{c2}. Black dots with error bars correspond to data, the solid blue lines are the overall fit results, dashed red lines represent signal contributions, and dashed green lines are the fitted backgrounds.

TABLE I. BFs of $\chi_{cJ} \to \Sigma^-\bar{\Sigma}^+$ (in units of 10^{-5}), where the errors are statistical only. The statistical errors of the MC-determined efficiencies are negligible.

Quantity	χ_{c0}	χ_{c1}	χ_{c2}
$N^{\rm obs}$	2143 ± 102	214 ± 53	131 ± 51
Efficiency $(\epsilon)\%$	9.56	8.58	6.97
$\mathcal{B}(\psi(3686) \to \gamma\chi_{cJ})\%$	9.79	9.75	9.52
$\mathcal{B}(\chi_{cJ} \to \Sigma^-\bar{\Sigma}^+)(10^{-5})$	51.3 ± 2.4	5.7 ± 1.4	4.4 ± 1.7

TABLE II. Systematic uncertainties in the BF measurements in percent.

Source	χ_{c0}	χ_{c1}	χ_{c2}
MDC Tracking	2.8	2.8	2.8
Photon Reconstruction	1.0	1.0	1.0
Kinematic Fit	5.8	5.8	5.8
π^0 mass window	1.6	–	–
$\pi^+\pi^-$ mass window	0.6	–	–
$M_{\rm rec}(\pi^+\pi^-)$ mass window	1.0	–	–
Bin size of Σ^-;	0.3	1.0	1.5
Signal Shape	2.6	2.8	0.0
Background Shape	1.2	2.9	3.2
Fitting Range	1.0	2.5	4.3
Signal Shape of χ_{cJ};	0.0	0.0	0.0
Background Shape	0.0	1.4	1.6
Fitting Range	0.2	1.8	2.3
Generator	–	4.2	4.1
Truth Match	0.7	0.7	0.7
Number of $\psi(3686)$	0.6	0.6	0.6
$\mathcal{B}(\psi(3686) \to \gamma\chi_{cJ})$	2.0	2.5	2.1
Total	7.9	9.8	10.2

(i) Bin Width: The bin width in the bin-by-bin fit is determined to be 10 MeV/c^2 by testing a series of MC samples as described in Sec. IV. The systematic uncertainties are determined by taking the difference between the determined branching fractions and their input values for $\chi_{cJ} \to \Sigma^-\bar{\Sigma}^+$.

(ii). Fit of χ_{cJ}: To extract the uncertainties associated with the fit procedure on $M_{\rm rec}(\gamma)$, alternative fits are performed by replacing the second-order polynomial function with a third-order function for the background description, fixing the width of the Gaussian functions for the signal description, and by varying the fitting range. All the relative changes in the results are taken as the uncertainties from the fit.

(iii) Fit of $M(\Sigma^-)$: Similarly, alternative fits are applied by varying the MC-simulated signal and background shapes and fit ranges. The differences are treated as a systematic uncertainty.

f. Generator: For the χ_{c0} case, the angular distribution of the Σ^- in the χ_{c0} rest frame is isotropic since the χ_{c0} is a scalar particle. Therefore, no systematic uncertainty needs to be considered for the χ_{c0}. For $\chi_{c1,2}$, on the other hand, we considered two extreme cases in the analysis, namely with $\alpha = 1$ and -1, respectively. The resulting differences in efficiency with a factor of $\sqrt{12}$ are then assigned as the source of a systematic uncertainty.

g. MC Truth Matching Angle: Since in the analysis of the signal MC data sample only events are selected whereby the difference between the angle of the reconstructed photon and the generated one (MC truth angle) is less than 10°, it might lead to a systematic error in the efficiency determination. Several differences with MC truth angles are considered ranging from 10° to 20°. The largest difference on the efficiencies are considered as the source of systematic uncertainty.

Other Uncertainties: The total number of $\psi(3686)$ decays is determined by analyzing the inclusive hadronic events from $\psi(3686)$ decays with an uncertainty of 0.6% [15]. The uncertainties due to the BFs $\psi(3686) \to \gamma\chi_{cJ}$ are quoted from the PDG [1]. The systematic error due to uncertainties in the trigger efficiency is negligible for this analysis.

Total Systematic Uncertainty: We assume that all systematic uncertainties given above are independent and we add them in quadrature to obtain the total systematic uncertainty.

TABLE III. Results of the BFs (in units of 10^{-5}) for the measurement of $\chi_{cJ} \to \Sigma^-\bar{\Sigma}^+$, compared with the $\chi_{cJ} \to \Sigma^+\bar{\Sigma}^-$ results from BESIII [13] and theoretical predictions [4][5][11]. The first errors are statistical and the second systematic.

Channel	This work	Statistical significance	BESIII [13]	Theoretical predictions	
	$\chi_{cJ} \to \Sigma^-\bar{\Sigma}^+$		$\chi_{cJ} \to \Sigma^+\bar{\Sigma}^-$	COM	QCM [11]
$\chi_{c0} \to \Sigma^-\bar{\Sigma}^+$	$51.3 \pm 2.4 \pm 4.1$	$30\,\sigma$	$50.4 \pm 2.\ 5 \pm 2.7$	5.9-6.9 [5]	18.1 ± 3.9
$\chi_{c1} \to \Sigma^-\bar{\Sigma}^+$	$5.7 \pm 1.4 \pm 0.6$	$5.8\,\sigma$	$3.7 \pm 0.6 \pm 0\ .2$	3.3 [4]	...
$\chi_{c2} \to \Sigma^-\bar{\Sigma}^+$	$4.4 \pm 1.7 \pm 0.5$	$3.6\,\sigma$	$3.5 \pm 0.7 \pm 0\ .3$	5.0 [4]	4.3 ± 0.4

VI. SUMMARY

Based on $(448.1 \pm 2.9) \times 10^6\,\psi(3686)$ events collected with the BESIII detector, the BFs of the processes $\chi_{cJ} \to \Sigma^-\bar{\Sigma}^+$ are measured and the results are summarized in Table III. This is the first BF measurement of $\chi_{cJ} \to \Sigma^-\bar{\Sigma}^+$. The results of $\chi_{cJ} \to \Sigma^-\bar{\Sigma}^+$ are consistent with $\chi_{cJ} \to \Sigma^+\bar{\Sigma}^-$ [13] from BESIII within the uncertainties, which confirm the prediction of isospin symmetry. The BF of $\chi_{c0} \to \Sigma^-\bar{\Sigma}^+$ does not vanish, which demonstrates a strong violation of the HSR. Both predictions based on the COM [5] and QCM [11] fail to describe our measured result. The measured BFs of $\chi_{c1,2} \to \Sigma^-\bar{\Sigma}^+$ are in good agreement with the theoretical predictions based on COM [4] and consistent within 1σ with the prediction based on QCM [11] for $\chi_{c2} \to \Sigma\Sigma$.

ACKNOWLEDGMENTS

The BESIII collaboration thanks the staff of BEPCII and the IHEP computing center and the supercomputing center of USTC for their strong support. This work is supported in part by National Key Basic Research Program of China under Contract No. 2015CB856700; National Natural Science Foundation of China (NSFC) under Contracts Nos. 11625523, 11635010, 11735014, 11822506, 11835012, 11935015, 11935016, 11935018, 11961141012, 11335008, 11375170, 11475164, 11475169, 11625523, 11605196, 11605198, 11705192; the Chinese Academy of Sciences (CAS) Large-Scale Scientific Facility Program; Joint Large-Scale Scientific Facility Funds of the NSFC and CAS under Contracts Nos.U1732263, U1832207, U1532102, U1832103; CAS Key Research Program of Frontier Sciences under Contracts Nos. QYZDJ-SSW-SLH003, QYZDJ-SSW-SLH040; 100 Talents Program of CAS; INPAC and Shanghai Key Laboratory for Particle Physics and Cosmology; ERC under Contract No. 758462; German Research Foundation DFG under Contracts Nos. Collaborative Research Center CRC 1044, FOR 2359; Istituto Nazionale di Fisica Nucleare, Italy; Ministry of Development of Turkey under Contract No. DPT2006K-120470; National Science and Technology fund; STFC (United Kingdom); The Knut and Alice Wallenberg Foundation (Sweden) under Contract No. 2016.0157; Olle Engkvist Foundation (Sweden); The Royal Society, UK under Contracts Nos. DH140054, DH160214; The Swedish Research Council; U. S. Department of Energy under Contracts Nos. DE-FG02-05ER41374, DE-SC-0012069.

[1] M. Tanabashi *et al.* (Particle Data Group), Phys. Rev. D **98**, 030001 (2018).
[2] M. Ablikim *et al.* (BESIII Collaboration), Chin. Phys. C **44**, 040001 (2020).
[3] G. T. Bodwin, E. Braaten, and G. P. Lepage, Phys. Rev. D **51**, 1125 (1995); J. Bolz, P. Kroll, and G.A. Schuler, Phys. Lett. B **392**, 198 (1997).
[4] S. M. H. Wong, Eur. Phys. J. C **14**, 643 (2000).
[5] X. H. Liu and Q. Zhao, J. Phys. G **38**, 035007 (2011).
[6] J. Z. Bai *et al.* (BES Collaboration), Phys. Rev. Lett. **81**, 3091 (1998).
[7] M. Ablikim *et al.* (BESIII Collaboration), Phys. Rev. D **87**, 032007 (2013), Erratum: Phys. Rev. D **87**, 059901 (2013).
[8] S. J. Brodsky, and G. P. Lepage, Phys. Rev. D **24**, 2848 (1981).
[9] V. L. Chernyak and A. R. Zhitnitsky, Phys. Rept. **112**, 173 (1984).
[10] M. Ablikim *et al.* (BES Collaboration), Phys. Rev. D. **73**, 052006 (2006).
[11] R. G. Ping, B. S. Zou, and H. C. Chiang, Eur. Phys. J. A **23**, 129 (2004).
[12] P. Naik *et al.* (CLEO Collaboration), Phys. Rev. D. **78**, 031101 (2008).
[13] M. Ablikim *et al.* (BESIII Collaboration), Phys. Rev. D. **97**, 052011 (2018).
[14] X. H. Liu and Q. Zhao, Phys. Rev. D **81**, 014017 (2010).
[15] M. Ablikim *et al.* (BESIII Collaboration), Chin. Phys. C. **42**, 023001(2018).
[16] M. Ablikim *et al.* (BESIII Collaboration), Nucl. Instrum. Meth. A **614**, 345 (2010).
[17] S. Agostinelli *et al.* (GEANT4 Collaboration), Nucl. Instrum. Meth. A **506**, 250 (2003).
[18] S. Jadach, B. F. L. Ward and Z. Was, Phys. Rev. D **63**, 113009 (2001); Comput. Phys. Commun. **130**, 260 (2000).
[19] D. J. Lange, Nucl. Instrum. Meth. A **462**, 152 (2001); R. G. Ping, Chin. Phys. C **32**, 599 (2008).
[20] J. C. Chen, G. S. Huang, X. R. Qi, D. H. Zhang and Y. S. Zhu, Phys. Rev. D **62**, 034003 (2000); R. L. Yang,

R. G. Ping and H. Chen, Chin. Phys. Lett. **31**, 061301 (2014).

[21] W. M. Tanenbaum *et al.*, Phys. Rev. D. **17**, 1731 (1978); G. R. Liao, R. G. Ping, and Y. X. Yang, Chin. Phys. Lett. **26**, 051101 (2009).

[22] Due to the unknown polarization in the production of Σ^- and small value of asymmetry parameters, $\alpha = 0.068$ [1], the efficiency difference between PHSP and differential helicity amplitude can be neglected.

[23] M. Ablikim *et al.* (BESIII Collaboration), Phys. Rev. D **86**, 032014 (2012).

[24] X. Zhou, S. Du, G. Li and C. Shen, arXiv:2001.04016 [hep-ex].

[25] M. Ablikim *et al.* (BESIII Collaboration), Phys. Rev. D **83**, 012006 (2011).

[26] R. Wanke, *Data Analysis in High Energy Physics*, (Wiley-VCH Verlag GmbH and Co. KGaA, 2013) pp. 263-280.